# Direct and Retrograde Wave Propagation in Unidirectionally Coupled Wilson-Cowan Oscillators

Guy Elisha,[1,*] Richard Gast,[2,*,†] Sourav Halder,[3,4] Sara A. Solla,[2,5] Peter J. Kahrilas,[3,4] John E. Pandolfino,[3,4] and Neelesh A. Patankar[1,‡]

[1]Department of Mechanical Engineering, Northwestern University, Evanston, Illinois, USA
[2]Department of Neuroscience, Feinberg School of Medicine, Northwestern University, Evanston, Illinois, USA
[3]Division of Gastroenterology and Hepatology, Feinberg School of Medicine, Northwestern University, Evanston, Illinois, USA
[4]Kenneth C. Griffin Esophageal Center, Feinberg School of Medicine, Northwestern University, Evanston, Illinois, USA
[5]Department of Physics and Astronomy, Northwestern University, Evanston, Illinois, USA

(Received 17 March 2024; revised 19 September 2024; accepted 11 December 2024; published 6 February 2025)

Some biological systems exhibit both direct and retrograde propagating signal waves despite unidirectional coupling. To explain this phenomenon, we study a chain of unidirectionally coupled Wilson-Cowan oscillators. Surprisingly, we find that changes in the homogeneous global input to the chain suffice to reverse the wave propagation direction. To obtain insights, we analyze the frequencies and bifurcations of the limit cycle solutions of the chain as a function of the global input. Specifically, we determine that the directionality of wave propagation is controlled by differences in the intrinsic frequencies of oscillators caused by the differential proximity of the oscillators to a homoclinic bifurcation.

DOI: 10.1103/PhysRevLett.134.058401

Coupled oscillators models have been successful in describing biological processes [1,2]. In particular, chains of coupled oscillators have been used to model animal behavior such as crawling, swimming, and peristalsis [3–8]. Previous studies of the properties of these models have focused on synchronization, phase locking, and the direction of wave propagation [9–12]. In chains of coupled oscillators, phase lags between adjacent oscillators yield a propagating wave [13,14]. The magnitude and sign of this phase lag appears to play a key role in controlling the dynamics and behavior of biological systems. For instance, phase lags have been reported to control the direction and speed of muscle contractions in organs [15–17], cognitive processes [18–20], and locomotion [21–23].

Switching between direct (from proximal to distal) and retrograde (from distal to proximal) wave propagation can facilitate flexible adaptation to environmental demands [24–30]. However, a switch in the direction of wave propagation can also indicate a dysfunction [31,32]. In esophagology, the question of how the direction of propagation can switch in a unidirectionally coupled chain of oscillators remains unanswered [32]. Revealing the mechanisms that control the direction of wave propagation in coupled oscillator systems can thus improve our understanding of a large family of biological systems [32,33].

Here, we focus on a chain of unidirectionally coupled limit cycle oscillators, a relevant model in many biological settings [6,21,34–37]. For example, sustained volumetric esophageal distension triggers stretch receptors along the distended region. These receptors are simultaneously triggered, stimulating local excitatory neurons. Empirically, a chain of unidirectionally coupled relaxation oscillators is deemed an appropriate model for the esophagus [38,39].

Coupled oscillators models capable of producing both direct and retrograde propagating waves have previously been studied to model biological systems [34,40–42]. Studying crawling in Drosophila larvae via a bidirectionally coupled chain of oscillators, Gjorgjieva *et al.* [40] obtained a direct wave when applying a stimulating input to only the anterior (proximal) oscillator, and a retrograde wave when applying an input to only the posterior (distal) oscillator. Thus, switching the direction of wave propagation required switching a localized input from the proximal to the distal oscillator. Other studies suggested that transitions in the direction of wave propagation occur through changes in the local intrinsic frequency of oscillation, a mechanism that can be implemented through frequency gradients, external perturbations, or varying local inputs [34,42–46]. Varying the strength and orientation of the couplings along the chain has also been shown to influence the direction of wave propagation [13,14,42]. However, the biological implementation of these mechanisms would place the system under strong demands that might not be met under normal operational conditions. For example, changing the synaptic coupling within a neural population is a slow process in comparison to the speed of propagation

*These authors contributed equally to this work.
†Present address: Dorris Neuroscience Center, The Scripps Research Institute, San Diego, California, USA.
‡Contact author: n-patankar@northwestern.edu

 

of traveling waves in the brain; it would be challenging to implement coupling adjustments fast enough to match the timescale of changing behavioral demands [47].

In this Letter, we identify and explain a novel mechanism for reversing the wave propagation direction in a chain of unidirectionally coupled limit cycle oscillators. This mechanism depends only on changes in an homogeneous global input and does not require any tuning of system coupling or of local inputs. Instead, changes in the global extrinsic drive to the chain of oscillators suffice to control the direction of wave propagation. The ability of this mechanism to operate on timescales as fast as the neural activity itself suggests that it could dynamically emerge in a variety of biological systems beyond the esophagus.

We consider a chain of unidirectionally coupled Wilson-Cowan (WC) oscillators [40,48] [see Fig. 1(a)]. The evolution of excitatory ($E$) and inhibitory ($I$) activities in this synaptically coupled neuronal network is described by

$$\tau_E \dot{E}_i = -E_i + (1 - E_i)\sigma_E[aE_i + bE_{i-1} - eI_i - dI_{i-1} + S_E], \tag{1}$$

$$\tau_I \dot{I}_i = -I_i + (1 - I_i)\sigma_I[cE_i - fI_i + S_I], \tag{2}$$

where the subscript $i$ identifies the $i$th oscillator, with $i = 1, \ldots, N$. We identify $i = 1$ and $i = N$ as the proximal and distal end oscillators, respectively; $\tau_E$ and $\tau_I$ are time constants. The parameters $a$–$f$ represent the average number of synapses per cell in the respective populations. Synaptic coupling between neighboring oscillators is realized via $b$ and $d$, which represent the number of synapses from the excitatory and inhibitory populations of an oscillator to the excitatory population of the subsequent oscillator in the chain [40]. The first oscillator receives no input from the network, i.e., $b = d = 0$ at $i = 1$, making it the only decoupled oscillator. The activation functions $\sigma_E$ and $\sigma_I$ are chosen as sigmoids of the form [48]

$$\sigma_{E/I}[x] = \frac{1}{1 + \exp[-\lambda_{E/I}(x - \phi_{E/I})]} - \frac{1}{1 + \exp(\lambda_{E/I}\phi_{E/I})}. \tag{3}$$

These represent the nonlinear response of the neural populations to a ramp input current [49]. The parameters $\lambda$ and $\phi$ are the activation rate and the activation threshold, respectively. Note that $\sigma_{E/I}[x = 0] = 0$. Finally, the system is driven by $S_E$ and $S_I$, which are extrinsic inputs globally applied to all excitatory and inhibitory populations, respectively. The default values of all model parameters are provided in Table I [39,40,48].

To ensure that stable limit cycle solutions exist for the parameter values used here, we performed a bifurcation analysis of a *decoupled* oscillator described by Eqs. (1) and (2) with $b = d = 0$. We used the parameter continuation software PYCOBI [51] to numerically obtain solutions of the WC equations as a function of the inputs $S_E$ and $S_I$. The bifurcation structure of the system in the 2D parameter space spanned by $S_E$ and $S_I$ [see Fig. 1(c)] is organized by two Bogdanov-Takens bifurcations that give rise to fold

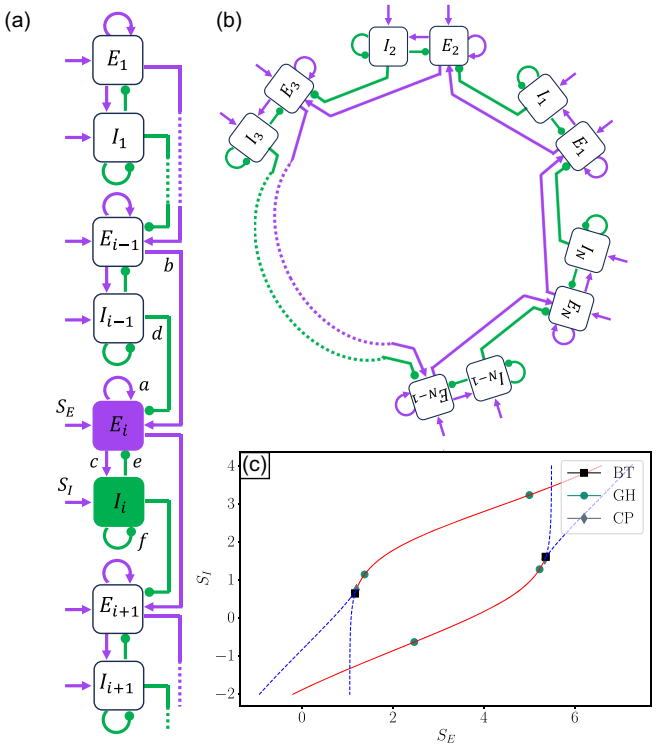


FIG. 1. Schematic of the model and its phase diagram. The neural network is a chain of $N$ unidirectionally coupled relaxation oscillators, each consisting of excitatory ($E$) and inhibitory ($I$) neural populations. Purple lines denote excitatory synapses and green lines denote inhibitory synapses. (a) Chain configuration. Neuronal connections $a$–$f$ are labeled for segment $i$. Uniform external inputs are $S_E$ and $S_I$. (b) Ring configuration. (c) Phase diagram of the proximal, isolated oscillator. For the phase diagram of an oscillator within the ring, see Figs. S3–S5 in [50]. BT, Bogdanov-Takens bifurcation; GH, generalized Hopf bifurcation; CP, cusp bifurcation; dashed blue lines, fold bifurcation curves; solid red lines, Hopf bifurcation curves.

TABLE I. Model parameters and their values.

| Symbol | Value | Symbol | Value | Symbol | Value |
|---|---|---|---|---|---|
| $a$ | 16 | $f$ | 3 | $\phi_E$ | 4 |
| $b$ | 20 | $S_E$ | 1.14 to 5.27[a] | $\phi_I$ | 3.7 |
| $c$ | 12 | $S_I$ | −1.31 to 2.46[b] | $\lambda_I$ | 2 |
| $d$ | 40 | $\lambda_E$ | 1.3 | $\tau_I$ | 4 |
| $e$ | 15 | $\tau_E$ | 1 | | |

[a]The $S_E$ parameter takes values within a range defined by the phase diagram in Fig. 1(c).
[b]The $S_I$ parameter takes values within a range defined by the phase diagram in Fig. 1(c).

and Hopf bifurcation curves [52]. In the vicinity of the Bogdanov-Takens bifurcation, the system dynamics are governed by a stable fixed point and an unstable saddle point, which collide in a fold bifurcation. Additionally, a limit cycle emerges from the stable fixed point through an Andronov-Hopf bifurcation. The existence of this limit cycle is bounded by the saddle point curves; the limit cycle disappears through a saddle homoclinic bifurcation. Global inputs $S_E$ and $S_I$ are chosen so that the system dynamics remain in the region enclosed by the fold (blue) and Hopf (red) bifurcation lines in Fig. 1(c), where stable oscillations exist.

We obtain our results from numerical simulations of a chain of $N = 70$ WC oscillators subject to systematic changes in the global input parameters $S_E$ and $S_I$. For each combination of inputs within the oscillatory regime, we find that the network converges to a synchronized state where all oscillators display phase locked dynamics [Figs. 2(a) and 2(b)]. The steady-state oscillation frequency of the chain (period $T_S$) is identical to the intrinsic frequency of a decoupled oscillator. Since the only decoupled oscillator in the chain is the proximal one, the frequency of each oscillator in the chain converges to that of the proximal oscillator. During the transient, the distal part of the chain exhibits nearly synchronized oscillations [Figs. 2(a) and 2(b)] at a frequency (period $T_R$) that differs from the steady-state frequency (period $T_S$). Depending on the values of $S_E$ and $S_I$, the stable phase lag between adjacent oscillators along the chain is positive or negative, resulting in retrograde or direct wave propagation, respectively. For example, Figs. 2(a) and 2(b) show that, for $S_I = 0$, decreasing $S_E$ results in a reversal of the wave direction from direct to retrograde.

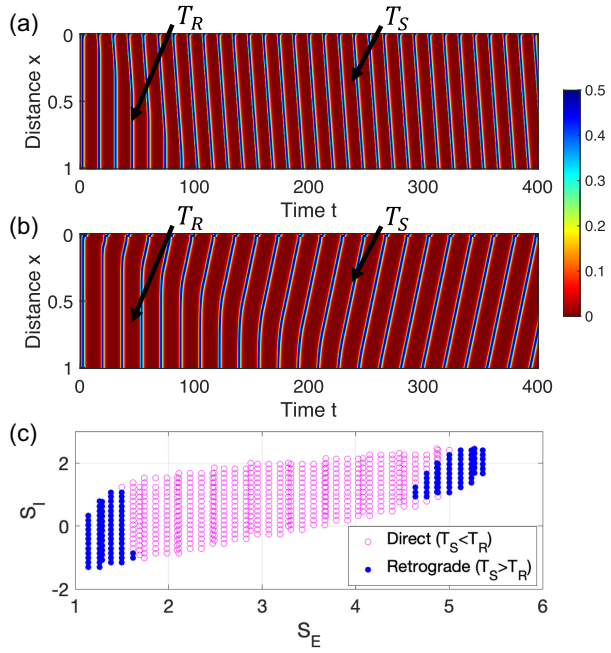


FIG. 2. Spatiotemporal dynamics and phase transitions. (a),(b) Spatiotemporal dynamics of the fast variable $E$ for $S_E = 2$, $S_I = 0$ (a), and for $S_E = 1.4$, $S_I = 0$ (b). The variable $x$ is the normalized distance to the proximal oscillator; $x = 0$ corresponds to $i = 1$ and $x = 1$ corresponds to $i = N$. Time is measured in arbitrary units set by $\tau_E = 1$. Values of all other parameters are reported in Table I. (c) Propagation direction along a chain is determined by the sign of $T_S - T_R$. Both $T_S$ and $T_R$ correspond to the limit cycle solution of Eq. (4), with $a^* = a = 16$, $e^* = e = 15$ for the chain's isolated (decoupled) oscillator, and $a^* = 36$ and $e^* = 55$ for a ring's typical oscillator.

How can a change in the value of a global input [$S_E$ in Figs. 2(a) and 2(b)] cause a reversal in the phase lag between adjacent oscillators? To shed light on this, we first investigate whether a similar behavior manifests in the ring configuration depicted in Fig. 1(b). The ring configuration has a periodic boundary condition, wherein the first oscillator ($i = 1$) receives input from the last oscillator ($i = N$), and Eq. (1) for $i = 1$ follows from setting $i - 1 = N$, with $b$ and $d$ no longer set to zero. We find that all oscillators in the ring oscillate not only at the same frequency (period $T_R$) but also at the same phase, independent of the choice of $S_E$ and $S_I$ within the range of values that elicit oscillations (see Fig. S6 in [50]).

To describe the global oscillation of the ring, we used a single WC oscillator with the parameters in Eq. (1) replaced by effective parameters ($a^* = a + b, b^* = 0, d^* = 0, e^* = e + d$) to obtain

$$\tau_E \dot{E}_i = -E_i + (1 - E_i)\sigma_E[a^* E_i - e^* I_i + S_E]. \quad (4)$$

For given values of the global inputs $S_E$ and $S_I$, ring oscillators converge to an intrinsic oscillation frequency that is identical to the transient frequency expressed by the distal chain oscillators (period $T_R$), but different from the intrinsic frequency (period $T_S$) of the proximal chain oscillator (see Fig. S7 in [50]).

Next, we discuss how these period differences between chain and ring network can explain the emergence of both direct and retrograde wave propagation in the chain. For sufficiently strong coupling, the first oscillator ($i = 1$), with an intrinsic oscillation period $T_S$, forces its adjacent neighbor to adjust its period from $T_R$ to $T_S$. This influence propagates down the chain, until the periods of all oscillators have converged to $T_S$ (see Fig. S7 in [50]). For $T_S < T_R$, chain oscillators below the proximal one are forced to speed up and a direct propagating wave emerges [see Fig. 2(a)]. For $T_S > T_R$, chain oscillators below the proximal one are forced to slow down and a retrograde propagating wave emerges [see Fig. 2(b)]. For $T_S = T_R$, a standing wave occurs (zero phase difference; see Fig. 4 in Appendix A). Changes in the period of the distal oscillator over time are shown for two scenarios in Fig. S7 in [50].

How can switches between these different wave propagation scenarios be triggered? Figure 2(c) shows that adjusting the global excitatory input $S_E$ suffices to reverse

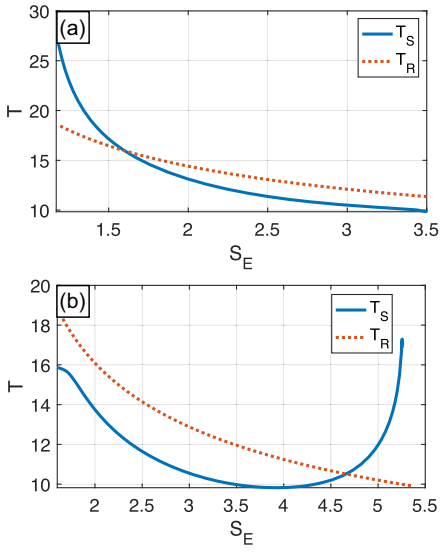


FIG. 3. Oscillation periods $T_R$ and $T_S$ as a function of global input $S_E$ for two different values of $S_I$. The intersection between the two curves indicates a reversal in propagation direction. (a) $S_I = 0.0$, (b) $S_I = 1.35$.

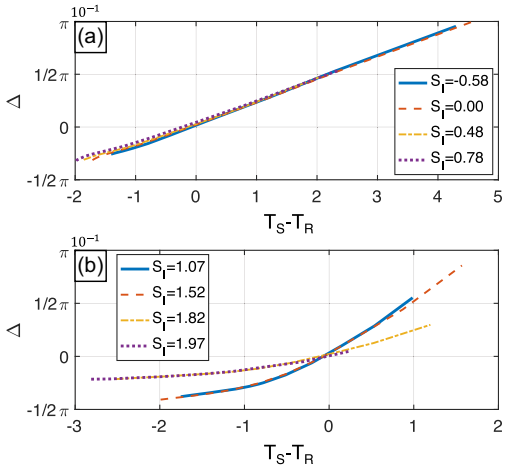


FIG. 4. Phase difference Δ between adjacent oscillators as a function of $T_S - T_R$ for various values of $S_I$. The sign of Δ determines the direction of propagation: direct for $\Delta < 0$ and retrograde for $\Delta > 0$. (a) For $S_E$ values less than 2.7, decreasing $S_E$ transforms a direct wave into a retrograde wave. (b) For $S_E$ values greater than 2.7, increasing $S_E$ eventually transforms a direct wave into a retrograde wave.

the direction of wave propagation, while the value of $S_I$ hardly plays a role. Two scenarios emerge, depending on the value of $S_E$. For large $S_E$, a strongly driven system, an additional *increase* in $S_E$ can change a direct wave into a retrograde wave. For small $S_E$, a weakly driven system, an additional *decrease* in $S_E$ can change a direct wave into a retrograde wave. Plots of $T_S$ and $T_R$ as a function of $S_E$ provide further insight onto switches in the direction of propagation. In Fig. 3(a), for $S_I = 0$ and small values of $S_E$, both $T_R$ and $T_S$ decrease monotonically with increasing $S_E$. A crossing at $T_S = T_R$ occurs because $T_S$ decreases more rapidly than $T_R$. This reflects the fact that the decoupled proximal oscillator is more strongly affected by the increase in the excitatory drive $S_E$; the effect of $S_E$ is not so strong in distal oscillators also driven by synaptic input. In Fig. 3(b), for $S_I = 1.35$ the switch occurs at a larger value of $S_E$. While $T_R$ again decreases monotonically with increasing $S_E$, the dependence of $T_S$ on $S_E$ is nonmonotonic. The increase of $T_S$ with $S_E$ beyond the minimum at around $S_E = 3.75$ results in a crossing at $T_S = T_R$. For additional insights on the occurrence of these crossings see Figs. S9 and S10 in [50], where we discuss the $E$ and $I$ nullclines of Eqs. (1) and (2).

The difference in how the oscillation frequency of proximal vs distal oscillators changes with $S_E$ can be explained by the bifurcation structure of the WC equations [Fig. 1(c)]. For the distal oscillators, the two Bogdanov-Takens bifurcations span a larger range on the $S_E$ axis than for the proximal one [see Fig. S8 in [50], where we draw a comparison between Figs. 1(c) and S5 in [50] ]. In the vicinity of the Bogdanov-Takens bifurcation, a homoclinic bifurcation of the limit cycle solution with a saddle point is guaranteed to exist [52]. As the limit cycle of a WC oscillator approaches such a homoclinic bifurcation, its period will grow toward infinity [53,54]. The difference in the effective parameters of the proximal vs the distal oscillators situates the proximal oscillator closer to the Bogdanov-Takens bifurcation point and thus closer to a homoclinic bifurcation of its limit cycle (see Fig. S8 in [50]). Changes in the uniform value of $S_E$ applied to the chain cause stronger changes in the oscillation period of the proximal oscillator as compared to all other oscillators (see Fig. 3); it is this difference that explains reversals in the direction of wave propagation (see Fig. 4).

In summary, we have shown that both direct and retrograde propagation can arise in a unidirectionally coupled chain of neural oscillators. In particular, we found that the direction of propagation is controlled by a disparity between the intrinsic frequency of the proximal oscillator and that of the more distal oscillators in the chain. This disparity is caused by differences in the input that the proximal vs the other oscillators receive from within the network. In the WC scenario, this difference explains the emergence of propagating waves that can be direct or retrograde. The transition between these two behaviors finds explanation in the proximity of the chain's operational regime to Bogdanov-Takens bifurcations. Neural systems have previously been proposed to operate close to a Bogdanov-Takens bifurcation. In this regime, slight alterations in the neural system's configuration can lead to significant shifts in its dynamics [55–58]. This proximity has been linked to phenomena like spike avalanches observed in cortical networks [58]. Our findings extend the range of applicability of this concept, revealing that the

proximity to a Bogdanov-Takens bifurcation also plays an important role for the dynamics that can emerge in coupled oscillator systems. We also note that the Bogdanov-Takens bifurcation is not specific to the WC model, but has been shown to exist in various neural population models [58–60]. Our Letter emphasizes the functional role that the existence of this bifurcation plays for activity propagation in neural systems.

Neuromodulators such as dopamine, serotonin, or acetylcholine can reliably cause such global, dynamic changes in the level of excitation [61]; we propose this as a self-organization mechanism that allows neural systems to flexibly react to changing behavioral demands without relying on slow plasticity related changes in synaptic couplings or intrinsic oscillator properties. Thus, this Letter not only provides insights into dysfunctional retrograde waves in organs such as the esophagus [32,39], but it could potentially lead to therapeutics based on neuromodulators to address the pathology.

Lastly, we discuss wave propagation in the context of phase oscillator networks that can be related to many different oscillatory systems through phase reductions (see Appendix B). We found a direct relationship between the differences in oscillatory periods $T_R$ and $T_S$ and the phase shift parameter of a phase coupling function, thus extending the numerical results we obtained in a neural oscillator model to a more general phase oscillator model. While the dynamic adjustments of phase relationships certainly plays a role in neural communication [46,62], it may also hold relevance in other areas such as robotics, where understanding how biological systems achieve efficient autonomous control is crucial for locomotion [21,63–65].

*Acknowledgments*—This work was funded by the by the National Institutes of Health (NIDDK Grant No. DK079902 and No. DK117824), and National Science Foundation (OAC Grant No. 1931372). We thank a reviewer for suggesting the extension of our analysis to simplified phase oscillators.

G. E. and R. G. contributed equally to this work. G. E., N. A. P., R. G., and S. A. S. wrote the main manuscript text and prepared all the figures. G. E. wrote the code. G. E., R. G., S. A. S., and N. A. P. developed the mathematical formulation. G. E., N. A. P., R. G., S. A. S., S. H., J. E. P., and P. J. K. interpreted results. N. A. P., J. E. P., and P. J. K. obtained funding.

[1] A. T. Winfree, J. Theor. Biol. **16**, 15 (1967).
[2] S. H. Strogatz and I. Stewart, Sci. Am. **269**, 102 (1993).
[3] C. Pehlevan, P. Paoletti, and L. Mahadevan, eLife **5**, e11031 (2016).
[4] N. A. Trayanova, J. Constantino, and V. Gurev, Am. J. Physiol. **301**, H279 (2011).
[5] E. Daniel, B. Bardakjian, J. Huizinga, and N. Diamant, Am. J. Physiol. **266**, G339 (1994).
[6] J. J. Collins and I. N. Stewart, J. Nonlinear Sci. **3**, 349 (1993).
[7] H. Ji, A. D. Fouad, S. Teng, A. Liu, P. Alvarez-Illera, B. Yao, Z. Li, and C. Fang-Yen, eLife **10**, e69905 (2021).
[8] P. F. Rowat and A. I. Selverston, J. Neurophysiol. **70**, 1030 (1993).
[9] P. Ashwin, S. Coombes, and R. Nicks, J. Math. Neurosci. **6**, 1 (2016).
[10] M. A. Schwemmer and T. J. Lewis, in *Phase Response Curves in Neuroscience: Theory, Experiment, and Analysis* (Springer, New York, 2012), pp. 3–31.
[11] P. Strumiłło and M. Strzelecki, Int. J. Appl. Math. Comput. Sci. **16**, 513 (2006), https://bibliotekanauki.pl/articles/908378.pdf.
[12] A. H. Cohen, P. J. Holmes, and R. H. Rand, J. Math. Biol. **13**, 345 (1982).
[13] N. Kopell and G. B. Ermentrout, Chains of oscillators in motor and sensory systems, in *Handbook of Brain Theory and Neural Networks*, edited by M. Arbib (MIT Press, Cambridge, MA, 2003), 2nd ed., pp. 201–205, https://math.bu.edu/people/nk/papers.html.
[14] N. Kopell and G. B. Ermentrout, Commun. Pure Appl. Math. **39**, 623 (1986).
[15] R. L. Kirby, D. A. MacLeod, and A. E. Marble, Angiology **40**, 620 (1989).
[16] P. Du, G. O'Grady, J. B. Davidson, L. K. Cheng, and A. J. Pullan, Crit. Rev. Biomed. Eng. **38**, 225 (2010).
[17] A. Pullan, L. Cheng, R. Yassi, and M. Buist, Prog. Biophys. Molec. Biol. **85**, 523 (2004).
[18] F. Varela, J.-P. Lachaux, E. Rodriguez, and J. Martinerie, Nat. Rev. Neurosci. **2**, 229 (2001).
[19] R. Brette, PLoS Comput. Biol. **8**, e1002561 (2012).
[20] Francisco-Leandro P. Carlos, M.-M. Ubirakitan, Marcelo Cairrao Araujo Rodrigues, M. Aguilar-Domingo, E. Herrera-Gutiérrez, J. Gómez-Amor, M. Copelli, P. V. Carelli, and F. S. Matias, Phys. Rev. E **102**, 032216 (2020).
[21] A. J. Ijspeert, Neural Netw. **21**, 642 (2008).
[22] T. Matsushima and S. Grillner, J. Neurophysiol. **67**, 373 (1992).
[23] W. Friesen and R. Pearce, in *Seminars in Neuroscience* (Elsevier, New York, 1993), Vol. 5, pp. 41–47.
[24] F. S. Matias, L. L. Gollo, P. V. Carelli, S. L. Bressler, M. Copelli, and C. R. Mirasso, NeuroImage **99**, 411 (2014).
[25] R. M. Hutchison, T. Womelsdorf, E. A. Allen, P. A. Bandettini, V. D. Calhoun, M. Corbetta, S. Della Penna, J. H. Duyn, G. H. Glover, J. Gonzalez-Castillo *et al.*, NeuroImage **80**, 360 (2013).
[26] P. Stein, J. Neurophysiol. **34**, 310 (1971).
[27] C. L. Hughes and J. B. Thomas, Mol. Cell. Neurosci. **35**, 383 (2007).
[28] G. Haspel, M. J. O'Donovan, and A. C. Hart, J. Neurosci. **30**, 11151 (2010).
[29] M. Castedal, E. Björnsson, and H. Abrahamsson, Neurogastroenterol. Motil. **10**, 227 (1998).
[30] A. A. Gharibans, S. Kim, D. C. Kunkel, and T. P. Coleman, IEEE Trans. Biomed. Eng. **64**, 807 (2016).
[31] L. Lange, A. Vaeggemose, P. Kidmose, E. Mikkelsen, N. Uldbjerg, and P. Johansen, PLoS One **9**, e86775 (2014).
[32] D. A. Carlson, W. Kou, and J. E. Pandolfino, Neurogastroenterol. Motil. **32**, e13794 (2020).

[33] C. Bick, M. Goodfellow, C. R. Laing, and E. A. Martens, J. Math. Neurosci. **10**, 9 (2020).
[34] A. H. Cohen, G. B. Ermentrout, T. Kiemel, N. Kopell, K. A. Sigvardt, and T. L. Williams, Trends Neurosci. **15**, 434 (1992).
[35] E. M. Izhikevich, SIAM J. Appl. Math. **60**, 1789 (2000).
[36] F. K. Skinner and B. Mulloney, J. Neurosci. **18**, 3831 (1998).
[37] E. Ryzhii and M. Ryzhii, in *International Conference on Biomedical Informatics and Technology* (Springer, New York, 2013), pp. 67–75.
[38] T. I. Omari, A. Zifan, C. Cock, and R. K. Mittal, Am. J. Physiol. **323**, G145 (2022).
[39] G. Elisha, S. Halder, X. Liu, D. A. Carlson, P. J. Kahrilas, J. E. Pandolfino, and N. A. Patankar, arXiv:2402.18103.
[40] J. Gjorgjieva, J. Berni, J. F. Evers, and S. J. Eglen, Front. Comput. Neurosci. **7**, 24 (2013).
[41] S. K. Sarna, E. Daniel, and Y. Kingma, Am. J. Dig. Dis. **17**, 299 (1972).
[42] N. Kopell and G. B. Ermentrout, Math. Biosci. **90**, 87 (1988).
[43] R. Borisyuk, A. Khibnik, A. N. Balachandar, and J. Tabak, Phys. Rev. Res. **5**, 033017 (2023).
[44] S. M. Danner, S. D. Wilshin, N. A. Shevtsova, and I. A. Rybak, J. Physiol. **594**, 6947 (2016).
[45] A. Roxin and E. Montbrió, Physica (Amsterdam) **240D**, 323 (2011).
[46] H. Finger, R. Gast, C. Gerloff, A. K. Engel, and P. König, PLoS Comput. Biol. **15**, e1007551 (2019).
[47] C. O'Donnell, Curr. Opin. Neurobiol. **82**, 102778 (2023).
[48] H. R. Wilson and J. D. Cowan, Biophys. J. **12**, 1 (1972), https://www.cell.com/biophysj/fulltext/S0006-3495(72)86068-5.
[49] P. A. Robinson, C. J. Rennie, and J. J. Wright, Phys. Rev. E **56**, 826 (1997).
[50] See Supplemental Material at http://link.aps.org/supplemental/10.1103/PhysRevLett.134.058401 for direct and retrograde signal propagation in unidirectionally coupled Wilson-Cowan oscillators.
[51] R. Gast, T. R. Knösche, and A. Kennedy, PLoS Comput. Biol. **19**, e1011761 (2023).
[52] Y. A. Kuznetsov, *Elements of Applied Bifurcation Theory* (Springer Science & Business Media, New York, 2013).
[53] Y. Maruyama, Y. Kakimoto, and O. Araki, Biol. Cybern. **108**, 355 (2014).
[54] S. Gonchenko, A. Kazakov, D. Turaev, and A. L. Shilnikov, Chaos **32**, 010402 (2022).
[55] V. Buendía, P. Villegas, R. Burioni, and M. A. Muñoz, Phil. Trans. R. Soc. A **380**, 20200424 (2022).
[56] M. Forrester, J. J. Crofts, S. N. Sotiropoulos, S. Coombes, and R. D. O'Dea, Network Neurosci. **4**, 467 (2020), https://direct.mit.edu/netn/article/4/2/467/95823/The-role-of-node-dynamics-inshaping-emergent.
[57] T. Gross, Front. Neural Circuits **15**, 614268 (2021).
[58] M. Ehsani and J. Jost, J. Comput. Neurosci. **51**, 149 (2023).
[59] R. Gast, H. Schmidt, and T. R. Knösche, Neural Comput. **32**, 1615 (2020).
[60] R. Gast, S. A. Solla, and A. Kennedy, Proc. Natl. Acad. Sci. U.S.A. **121**, e2311885121 (2024).
[61] S.-H. Lee and Y. Dan, Neuron **76**, 209 (2012).
[62] G. Hahn, A. Ponce-Alvarez, G. Deco, A. Aertsen, and A. Kumar, Nat. Rev. Neurosci. **20**, 117 (2019).
[63] P. Ramdya and A. J. Ijspeert, Sci. Rob. **8**, eadg0279 (2023).
[64] V. Lobato-Rios, S. T. Ramalingasetty, P. G. Özdil, J. Arreguit, A. J. Ijspeert, and P. Ramdya, Nat. Methods **19**, 620 (2022).
[65] D. Drotman, S. Jadhav, D. Sharp, C. Chan, and M. T. Tolley, Sci. Rob. **6**, eaay2627 (2021).
[66] H. Nakao, Contemp. Phys. **57**, 188 (2016).
[67] B. Pietras and A. Daffertshofer, Phys. Rep. **819**, 1 (2019).

## End Matter

*Appendix A: Phase shift between adjacent oscillators as a function of $T_S - T_R$*—Figures 4(a) and 4(b) offer insights into changes in the direction of wave propagation in response to changes in $S_E$, with $S_I$ held constant. These figures present plots of the steady-state phase difference $\Delta$ between adjacent oscillators as a function of $T_S - T_R$. The plots reveal a monotonic dependence of the magnitude of the phase on the difference between the two periods. The figures also demonstrate that for a fixed value of the input $S_I$ to the inhibitory population, adjusting the input $S_E$ to the excitatory population suffices to alter the direction of wave propagation. As expected, the reversal in the direction of propagation consistently occurs for $T_R = T_S$, unaffected by $S_I$.

*Appendix B: Generalization to coupled phase oscillators*—We have shown (i) that chains of unidirectionally coupled oscillators can support both direct and retrograde wave propagation, and (ii) that changes in the global input to the coupled oscillator system suffice to switch between wave propagation directions. Furthermore, we have demonstrated that this phenomenon is caused by intrinsic oscillation frequency differences that arise between the first, autonomous oscillator in the chain, and the following oscillators in the chain, which are synaptically coupled. To generalize our results, we phrase them in terms of the phase difference $\psi = \theta_1 - \theta_2$, where the phases $\{\theta_1, \theta_2\}$ of the first and second oscillators in the chain evolve according to

$$\dot{\theta}_1 = \omega_1, \tag{B1}$$

$$\dot{\theta}_2 = \omega_2 + Z(\theta_1 - \theta_2), \tag{B2}$$

with intrinsic frequencies $\{\omega_1, \omega_2\}$ and phase sensitivity function $Z(\psi)$. Adopting previous work on periodically forced oscillators [66,67], we write the evolution of $\psi$ as

$$\dot{\psi} = \delta + \epsilon\Gamma(\psi), \tag{B3}$$

where $\delta = \omega_1 - \omega_2$, $\epsilon$ represents the strength of periodic forcing, and $\Gamma$ is a $2\pi$-periodic function that captures the effect of the driving oscillator on the phase of the receiving oscillator. It has been previously shown that the strong parameter dependence of the phase sensitivity function for the Wilson-Cowan equations renders a general analytic treatment via the phase reduction method difficult [67]. Instead, we considered a network of simplified oscillators with sinusoidal phase coupling that can be investigated analytically. We established a correspondence between these analytic results and our main numerical results for the WC network (see S5 in [50]), thus extending our results to a broader family of phase oscillator models. Most importantly, we found (i) that there are stable steady-state solutions with $\psi > 0$ and $\psi < 0$, even for $\delta = 0$ (see S5.1 of [50]), and (ii) that the reversal of wave propagation direction in the Wilson-Cowan model, caused by changes in the global input $S_E$, can be related to a phase shift of the coupling function $\Gamma$ (see S5.2 of [50]).